HAL
open science

The M 4.5 Vallorcine (French Alps) earthquake of 8 September 2005 and its complex aftershock sequence

Julien Fréchet, François Thouvenot, Michel Frogneux, Nicolas Deichmann, Michel Cara

To cite this version:

Julien Fréchet, François Thouvenot, Michel Frogneux, Nicolas Deichmann, Michel Cara. The M 4.5 Vallorcine (French Alps) earthquake of 8 September 2005 and its complex aftershock sequence. Journal of Seismology, 2010, 15 (1), pp.43-58. 10.1007/s10950-010-9205-8 . hal-00617322

HAL Id: hal-00617322

https://hal.science/hal-00617322v1

Submitted on 27 Aug 2011

HAL is a multi-disciplinary open access archive for the deposit and dissemination of scientific research documents, whether they are published or not. The documents may come from teaching and research institutions in France or abroad, or from public or private research centers.

L'archive ouverte pluridisciplinaire **HAL**, est destinée au dépôt et à la diffusion de documents scientifiques de niveau recherche, publiés ou non, émanant des établissements d'enseignement et de recherche français ou étrangers, des laboratoires publics ou privés.

Manuscript
Click here to download Manuscript: Frechet_Vallorcine_2010_revised.doc Click here to view linked References

The M_W 4.5 Vallorcine (French Alps) earthquake of 8 September 2005 and its complex aftershock sequence

Julien Fréchet[1], François Thouvenot[2], Michel Frogneux[1], Nicolas Deichmann[3], Michel Cara[1]

[1] *Institut de Physique du Globe de Strasbourg (CNRS/UDS), EOST, Université de Strasbourg, 5 rue René Descartes, 67084 Strasbourg, France*

[2] *Laboratoire de Géophysique Interne et Tectonophysique (CNRS/UJF), Maison des Géosciences, BP 53, 38041 Grenoble cedex 9, France*

[3] *Schweizerischer Erdbebendienst, ETH Zürich, 8092 Zürich, Switzerland*

Corresponding author: J. Fréchet
E-mail: jfrechet@unistra.fr
Tel: +33 (0)3 68 85 03 55 Fax: +33 (0)3 68 85 01 25

First version – 31 March 2010
Revised – 4 August 2010

Keywords: 2005 Vallorcine earthquake - Aftershocks - Hypocenter relocation - Similar waveforms - Western Alps seismicity - Remuaz fault

Abstract

On 8 September 2005 a moderate M_W 4.5 earthquake occurred in the north-western Alps midway between Chamonix (France) and Martigny (Switzerland). The focal mechanism corresponds to a right-lateral strike-slip on a N60°E fault plane. The foreshock–mainshock–aftershock sequence is investigated on the basis of data recorded by a temporary network of 28 stations deployed for one month just after the mainshock, and data from permanent, regional seismic networks. Absolute and relative locations of more than 400 events are obtained with a mean uncertainty of approximately 0.2 km. Small foreshocks, the mainshock and early and late aftershocks are located relative to the main aftershock set. The seismic sequence exhibits a surprisingly complex structure, with at least five clusters on distinct fault planes. The main elongated cluster agrees with the location of the mainshock, its hypocentre being 4.3 km below sea level. We discuss the relationship between the right-lateral fault beneath the Loriaz peak (the source of the Vallorcine event), the nearby normal Remuaz fault, and the regional seismotectonic stress field.

1 Introduction

The Vallorcine earthquake (M_W 4.5, M_L 4.9) occurred on 8 September 2005 at 11:27 UTC in the French Alps near the Swiss border (Fig. 1). Its epicentre was located in the Aiguilles Rouges massif, some 10 km north of Chamonix and the Mont Blanc massif. Though widely felt, it produced only slight damage in the epicentral zone, with a maximum intensity of V on the EMS-98 scale (BCSF 2005; Cara et al. 2007). Just one century earlier, on 29 April 1905, this zone was hit by the Chamonix earthquake, which caused significant damage, with a magnitude M_W = 5.5–5.6 and a maximum intensity VII–VIII MSK64 (Alasset 2005; Cara et al. 2008). A few kilometres to the southwest another earthquake causing slight damage occurred on 11 March 1817 (M_W = 4.8) with a maximum intensity VII MSK64 (ECOS 2009; SisFrance 2010). The Aiguilles Rouges massif is located at the western end of the Rhone fault zone in the Swiss Valais, one of the seismically active regions of the western Alps (Maurer et al. 1997; Pfiffner et al. 1997). Five historical earthquakes causing severe damage and reaching intensity VIII on the EMS-98 scale have occurred in the Valais over the last five centuries (ECOS 2009): Ardon (April 1524, M_W = 6.4), Aigle (11 March 1584, M_W = 6.4), Brig (9 December 1755, M_W = 6.1), Visp (25 July 1855, M_W = 6.4), and Ayent (25 January 1946, M_W = 6.1). On the French side, the level of historical seismic activity is lower, with a maximum intensity VII–VIII for two events only, while on the Italian side the level is even lower with only one known event exceeding intensity VI (at Pont-Saint-Martin on 5 March 1892, VII–VIII, M_W = 4.8). All known historical earthquakes with epicentral intensity above VI are plotted in Fig. 1. With the exception of the 1855 Visp and the 1892 Pont-Saint-Martin events, all the events are located in the external Alps, i.e. to the north-west of the Frontal Pennine Thrust, the major structural limit which represents the scar of the former Tethys in the north-western Alps.

The recent microseismicity as recorded by regional seismic networks is plotted in Fig. 1 for the period 1992–2004. Its distribution differs noticeably from the major historical earthquakes. The Frontal Pennine Thrust also appears today as a major boundary between different seismic domains. The external north-western zone exhibits a scattered seismicity throughout the domain, with a clear SW–NE alignment in the Valais. The internal south-

eastern zone exhibits a wide, elongated seismic zone following the Penninic front, a zone often called the Briançonnais seismic arc in the French section. The 1892 Pont-Saint-Martin earthquake lies within the south-easternmost seismic zone, called the Piedmontese seismic arc (Thouvenot and Fréchet 2005).

It has recently been demonstrated that the Briançonnais seismic arc corresponds to an extensional present-day stress regime, whereas the external zone is dominated by a strike-slip — or, more rarely, a compressional — regime (e.g. Maurer et al. 1997, Sue et al. 1999, Delacou et al. 2004, Kastrup et al. 2004, Thouvenot and Fréchet 2005). However, within the Aiguilles Rouges massif where the Vallorcine 2005 earthquake took place, the tectonic pattern could be more complex. A recent investigation of a Variscan fault, currently activated as a normal left-lateral fault on the eastern flank of the Aiguilles Rouges massif (the Remuaz fault) surmised that this fault might be responsible for the Chamonix 1905 earthquake (Alasset 2005; Alasset et al. 2005; Cara et al. 2006; Van der Woerd et al. 2006).

To obtain a detailed description of the fault segment that ruptured in 2005 and investigate its relation to the Mont Blanc – Aiguilles Rouges tectonics, we installed a temporary seismic network in the epicentral region the day after the Vallorcine event and operated it for about one month thereafter. This paper documents the numerous aftershocks recorded by the network, and analyses the complete foreshock–mainshock–aftershock sequence.

2 Mainshock

The Vallorcine mainshock occurred on 8 September 2005 at 11:27 UTC (13:27 local time). Its epicentre was located in the vicinity of Vallorcine, a village situated in the northern French Alps next to the Swiss border, at a distance of approximately 13 km from the two nearest large towns, Chamonix-Mont-Blanc (France) and Martigny (Switzerland). Its magnitude reached M_L 4.9 (after RENASS and SED, the French and Swiss national networks) and M_W 4.5±0.1 (Global CMT; SED 2005a, 2005b; Delouis et al., 2008, 2009). It was felt over a broad area with a radius of more than 200 km in the adjacent regions of France, Italy, and Switzerland. The maximum intensity reached a value of V EMS-98 with only slight

damage in the Vallorcine (France) – Martigny (Switzerland) area (BCSF 2005; Cara et al. 2007). It also triggered a number of rock falls in the Mont Blanc and Aiguilles Rouges massifs, one of them hurting a rock climber in the vicinity of Vallorcine. The earthquake affected springs in Vallorcine, inducing flow modifications, impurity content and a change in the colour of the water that persisted for several days.

2.1 Location

Preliminary locations provided by the French and Swiss agencies were all within 2 km of the village of Vallorcine (Table 1 and Fig. 2). As will be shown in a later section, the mainshock has been relocated by a joint hypocenter determination including foreshocks, mainshock and aftershocks. The procedure is based on the double-difference algorithm implemented in the HypoDD software (Waldhauser and Ellsworth 2000; Waldhauser 2001). Since many aftershocks were simultaneously recorded by the local temporary network and the permanent networks, station corrections related to velocity model uncertainties can be derived. These in turn allow the mainshock to be relocated relative to the well-located aftershocks. The resulting coordinates of the mainshock delivered by HypoDD are reported in Table 1. Its hypocenter is located at a depth of 4.3 km below sea level, corresponding to approximately 6.8 km below the surface. The hypocentre is thus located within the Aiguilles Rouges crystalline massif, 2.5 km west of Vallorcine, just below the Loriaz peak (Aiguille de Loriaz).

2.2 Focal mechanism

The focal mechanism of the mainshock was derived from the first-motion data recorded at 277 stations in France, Switzerland, Italy, Germany, Austria, and Slovenia. Epicentral distances range from 3 km (station EMV, Vieux-Emosson Reservoir) to 811 km (station ROSF, Brittany). The azimuthal coverage is good (Fig. 3), with a maximum gap of 14° in the NW quadrant. We used the focal position provided by the relocation procedure, and the Sellami et al. (1995) velocity model (8-layer crust with 38 km deep Moho). Out of the seismograms recorded in the 277 stations, we retained 222 polarities because of the low signal-to-noise ratio in the other 55 stations. The fault-plane solution is well constrained: changing the velocity model or the focal depth does not modify the strike and dip values of the nodal planes. However, a few discrepant observations can be noted in the southern azimuth; in the WSW azimuth (dilatation quadrant), two stations in the French Pyrenees inexplicably recorded clear compressions.

The mainshock had a pure strike-slip mechanism. The N60°E-striking nodal plane dips 65° to the SE, while the N150°E-striking plane is vertical. The N60°E direction corresponds to the main aftershock swarm as discussed in the next sections, which implies that motion on the N60°E-striking fault plane is right-lateral. Both the P- and T-axes plunge 18°. The P-axis trends WNW, and the T-axis NNE (Table 2). These results agree relatively well with the moment tensor derived from a full-waveform inversion of broad-band records, which gives a strike of 57°, a dip of 84°, and a rake of 178° for the nodal plane, based on 33 stations in Switzerland and neighbouring countries (Deichmann et al. 2006). Similar results were obtained by Delouis (2005) using only three French strong-motion stations in the 10–60 km distance and 178–324° azimuth ranges: strike 56°, dip 83°, rake 175°. The main difference between the first-motion and broad-band focal mechanisms is a higher 83-84° dip for the 56-60° striking plane. The seismic moment value given by the Swiss Seismological Service SED is $M_0 = 5.74 \times 10^{15}$ N·m and the moment magnitude $M_W = 4.47$ - exactly the same value as that found by Delouis et al. (2009). The seismic moment from the Global CMT catalogue is 9.34×10^{15} N·m ($M_W = 4.6$), with a nodal plane very similar to that obtained from first motions (strike 60°, dip 66°, rake 169°).

3 Data acquisition and processing

Beginning the day after the mainshock, we deployed 28 mobile stations in the epicentral zone (Fig. 2). This complete network was maintained for one month, while 4 stations were operated for an additional period of two and a half months. One station, 4 km from the epicentre, was kept operating even longer, until May 2006. The stations were installed and maintained by teams from the three participating geophysical institutes (IPGS in Strasbourg, LGIT in Grenoble, and SED in Zurich), and hence were rather heterogeneous. All stations were high-dynamic digital recorders equipped with three-component seismometers and GPS time receivers. Table 3 gives detailed information on the stations and sensors used.

During the one-month recording period starting on 9 September and ending on 10 October 2005, over 300 aftershocks were recorded, with magnitudes ranging from 2.4 (on 18 September) down to -0.7. As will be seen in the next section, 289 of these events were

recorded by a sufficiently large number of stations and could be precisely located. Given the heterogeneous recording systems, the original data were recorded in several different formats. During the first processing stage, all available data was converted into two common data formats, SAC (Seismic Analysis Code) and Sismalp, allowing us to create a homogeneous database. The temporary network had an extension of approximately 20 km. Two permanent stations are located within the temporary network (EMV—SED network—and OG03—Sismalp network—), while nine other permanent stations are located within 50 km of the temporary network and the mainshock epicentre (OG01,OG02, OG04, and RSL from the Sismalp/Rénass network, AIGLE, DIX, GRYON, SALAN, and SENIN from the SED network). The seismograms of these 11 permanent stations were merged with the data of the 28 temporary stations.

All recorded events were then picked using the Pickev2000 software (Fréchet and Thouvenot 2004). A total of 9630 P and S arrival times were read, along with over 1600 duration readings used for magnitude estimates. We firstly located all the events using the Hypref program (Fréchet 2005), an improved version of Hypo71 (Lee and Lahr 1975). Hypref handles higher time precision (millisecond accuracy), computes travel times taking into account station elevations, and allows users to specify the lowest turning-point layer reached by the ray (a feature enabling secondary arrivals to be processed, but which was not used here).

A second dataset was prepared in the same way, adding the four foreshocks that occurred on 3 and 5 September, the mainshock, and the first ten aftershocks recorded on 8 September. These 15 events were only recorded by the permanent networks. We also added the 100 late aftershocks that occurred between 11 October and 31 December 2005 to this dataset. The late aftershocks were recorded by both the permanent networks and the remaining one to five temporary stations. This heterogeneous dataset was then relocated in a second phase by means of the double-difference algorithm implemented in the HypoDD software (Waldhauser and Ellsworth 2000; Waldhauser 2001). This joint hypocenter relocation aims at two different goals: 1) high-resolution relocation of aftershock clusters, and 2) relocation of the fore-, main- and early after-shocks.

For both location procedures (Hypref and HypoDD), several tests were performed in order to find the most effective velocity model and program parameters. Two very different

velocity models were compared: the first consisted of the Sellami et al. (1995) minimum 1-D model (8-layer crust with 38-km-deep Moho) used for the focal mechanism study above, and representing the optimal 1D-model for the western Alps. The second was a simple half-space with a P-velocity of 6 km/s. No significant change in absolute position or depth was found using either model, while cluster structure was better resolved with the simple one-layer model. P- and S-wave arrival times were used, assigning half-weight to the latter. With Hypref, we obtained a mean RMS of 0.050 s and average relative horizontal and vertical uncertainties (ERH and ERZ) of 0.2 km. With HypoDD, the mean RMS could be reduced to 0.019 s.

4 The aftershocks recorded by the temporary network

Figure 4 presents the absolute locations (Hypref) of the 289 aftershocks recorded by the full temporary network during its one-month deployment. The prominent feature is an elongated cluster of aftershocks with an azimuth of 60° (named C1), approximately 2.5 km long. This main cluster of aftershocks was the only one active during the first seven days after the mainshock (with one exception on day 4, see below); 78 events in this cluster occurred during the first week and 81 thereafter. On 15 September at 09:33, a second cluster C2 became active, located 1.5 km north-northwest of the main cluster and comprising a total of 105 events. Two other smaller clusters were activated 4 and 12 days after the mainshock. Cluster C3 located 5 km north-west of the main cluster comprises 20 events; it became active on 12 September at 10:20 with the only event in the first 7 days that was not located in the main cluster, the next event occurring on 20 September. Cluster C4 located between clusters C1 and C2 comprises 12 events with its first event occurring on 20 September at 06:44.

The transverse cross-section shown in Fig. 5 is computed along the azimuth 150°. On this section, the main cluster C1 is sub-vertical, slightly dipping to the south-east. It defines a fault patch, approximately 2.5 km long and 2 km deep, with its top at a depth of 3 km below sea level, i.e. 4.5 km beneath the mean ground surface. Clusters C2 and C4 are located at about the same depth as the main cluster C1, while cluster C3 is located a little deeper, at an average depth of 6 km below sea level.

A more detailed picture of the four clusters is obtained by processing the same dataset with the HypoDD program, which results in a high-resolution relocation of the hypocenters. Figure 6 shows a close-up of the clusters on a map and in a cross-section. In the map view (Fig. 6a), the main cluster C1 is a well-defined linear feature, but divided into two sub-clusters separated by a 0.5 km long gap. The longitudinal cross-section AA' (Fig. 6b) includes only the aftershocks that are in the 0.7 km wide box sketched on the map view (Fig. 6a). It shows that the main aftershock cluster comprises several sub-clusters or asperities. The map view also shows that the second cluster (C2) is resolved into two sub-clusters C2a and C2b, also clearly visible on the transverse cross-section BB' (Fig. 6c). The southernmost sub-cluster C2a defines a sharp sub-vertical alignment oriented N70°E. The northernmost one (C2b) is less well defined; however, based on the relocation of the later aftershocks between 11 October and 31 December (Fig. 7) and other cross-sections, it defines an alignment oriented N80°E gently dipping to the south. Time-wise, sub-cluster C2a was active mainly during the first 20 days, while later activity was concentrated in sub-cluster C2b. The two smaller clusters C3 and C4 are highly concentrated within 150 m diameter volumes and do not have any preferred orientation.

5 The foreshock–mainshock–aftershock sequence

In order to study the relationship of the events recorded by the temporary network, described in the previous section, to the four foreshocks, the mainshock and the ten early aftershocks preceding deployment of the temporary network, we merged all data into a single dataset, which was then reprocessed with the HypoDD software. The relocated foreshocks, mainshock and early aftershocks are shown in Fig. 7 with the aftershock clusters as background. The mainshock is located right in the middle of the main cluster C1, while the early aftershocks are scattered around the central and eastern part of this cluster. One early aftershock could be associated with the small cluster C4. Three out of the four foreshocks took place exactly at the mainshock hypocenter position on 3 September, i.e. 5 days before the mainshock. On the other hand, the fourth and last foreshock occurred on 5 September at the position of cluster C3, 5 km north-west of the mainshock.

Thus the temporal and spatial coincidence of the mainshock and cluster C1 as well as the strike and dip of fault defined by the hypocenter distribution of this cluster allow us to identify the N60°E nodal plane of the mainshock focal mechanism as the actual fault plane.

After the 10 October, most temporary stations were withdrawn. However, more than 100 late aftershocks were recorded by the few remaining temporary stations and the permanent stations. They were included in the complete foreshock–mainshock–aftershock dataset. The global HypoDD inversion allowed us to relocate 94 of the late aftershocks. The resulting hypocenters are also plotted in Fig. 7. They all occurred within the main cluster C1 and sub-cluster C2b.

The time history of activity is plotted in Fig. 8 as a time-section along line BB'. To assess whether the earthquake clusters active immediately before and after the Vallorcine event were also active in the years before and after 2005, we searched the Swiss Seismological Service (SED) database for additional events that could be associated to these clusters since 1991. Because of the poor azimuthal station distribution, the routine locations of the SED network are not precise enough for such an analysis. We have therefore resorted to an assessment of the signal similarities between events known to be associated to these clusters based on the HypoDD relocations and events recorded before September 2005 and after December 2005 at selected stations. The vertical components at stations EMV and SALAN were band-pass filtered between 1 and 20 Hz. Visual inspection of the filtered traces allowed us unequivocally to identify families of similar events, making computation of cross-correlations unnecessary (Fig. 9). The summary of events detected by the permanent network of the SED over different time periods and associated to each cluster is summarized in Table 4.

Due to the size of cluster C1 as well as the large number and magnitude range of the events, the signal character is somewhat heterogeneous. Nevertheless, as shown in Fig. 9a, there are families of similar earthquakes within this large cluster that constitute unequivocal evidence of repeated sporadic activity of cluster C1, dating at least as far back as the year 2001 and extending well into 2009. But the main activity of cluster C1 is clearly linked to the ML 4.9 mainshock and for the most part constitutes an aftershock activity that will probably persist beyond the year 2009.

Cluster C2, in contrast, is quite different. The activity of this cluster started several days after the mainshock and, although it was very active in September and October 2005, activity declined rapidly thereafter and seems to have come to a complete stop in late 2006. As shown by some representative seismogram examples in Fig. 9b, the signals of the events within each sub-cluster (C2a and C2b) exhibit a high degree of similarity, but differ somewhat between the two sub-clusters, so that they can be clearly distinguished. From this it is clear that the activity of cluster C2 started in sub-cluster C2a, located closer to the mainshock, and then moved to sub-cluster C2b located slightly more to the NW (this is also visible from the temporal evolution shown in Fig. 8). A causal relation between cluster C2 and the mainshock and aftershocks in cluster C1 is therefore very likely.

Only four of the 20 events in cluster C3 recorded by the temporary network were strong enough also to be detected by the permanent network of the SED. The signals of these events recorded at station EMV are nearly identical, not only among these four events, but also to three other events that occurred in 2000 as well as two events in 2006 and one in 2007. So in contrast to cluster C2, which was only active over a short time period after the Vallorcine mainshock, cluster C3 constitutes a site of ongoing sporadic activity. Moreover, given the distance of about 5 km from the mainshock and the fact that in 2005 it became active before the occurrence of the mainshock, a causal link between the two is not immediately evident, although the increased activity in September and October 2005 might not be entirely fortuitous.

The events associated to cluster C4 were too weak to be detected by the permanent network of the SED. However, the temporal evolution of the activity recorded by the temporary network, as shown in Fig. 8, indicates that the activity of this cluster was limited to a few weeks. This temporal coincidence together with its location in between clusters C1 and C2 suggests that the activity in cluster C4 was probably linked in some way to the Vallorcine mainshock.

6 Discussion and conclusions

From the evidence presented above, we have found that the Vallorcine earthquake corresponds to the rupture of a fault segment located beneath the Loriaz peak, thereafter named the Loriaz fault. The rupture area is approximately 2.5 x 2 km^2 if we identify it with the main cluster of aftershocks, which is consistent with the moment magnitude $M_W = 4.5$. For example, using the relation between moment magnitude and rupture area $\log(A) = 0.9\ M_W - 3.42$ given by Wells and Coppersmith (1994) for strike-slip earthquakes, this results in a value of 4.4 km^2. It was unexpected that a moderate earthquake of this magnitude could generate such a complex pattern of secondary faulting within the aftershock sequence involving five fault segments, the furthest being at a distance of 5 km from the mainshock segment. This may suggest that the Loriaz seismic zone is highly fractured, with no major fault involved. This observation agrees with the mapped surface faults sketched in Fig. 10 (after Ayrton et al. 1987). In the Aiguilles Rouges massif, numerous short fault segments are mapped, with lengths of less than 2 km and strikes in the N20°E-N70°E range, i.e. sub-parallel to oblique to the N23°E-striking Remuaz Fault.

At a distance of 40 and 70 km to the south-west of Vallorcine, two other earthquakes were studied by means of temporary networks in recent years (Fig. 1): the Grand-Bornand earthquake on 14 December 1994 (Fréchet et al. 1996) and the Epagny earthquake on 15 July 1996 (Thouvenot et al. 1998). The Epagny earthquake—M_L 5.3—had a strike-slip mechanism and produced a profuse and protracted aftershock sequence, with more than 1000 aftershocks lasting for several months, and even years, a feature resembling the Vallorcine aftershock sequence. In contrast, the Grand-Bornand earthquake—M_L 5.1—was followed by a surprisingly low activity, fewer than 20 small aftershocks. The Grand-Bornand event was located at a depth of 8 to 10 km and its focal mechanism involved strike-slip motion with a significant thrust component. The P-axes of the three events—Grand-Bornand, Epagny, and Vallorcine—are remarkably coherent, their azimuths ranging from 274° to 282°, and their plunges from 16° to 22°.

The strike of the Loriaz fault, N60°E, is well defined by the main aftershock cluster and perfectly agrees with the nodal plane from first motions (Fig. 3) or from Global CMT. However, the dip of the nodal plane obtained from the same methods, 65–66°, differs

significantly from the apparent dip of the aftershock cluster, which is close to 80°. Deichmann et al. (2006) and Delouis (2005) found a dip of 83–84° much closer to the dip of the aftershock cluster. The strike values they found (N57°E and N56°E respectively) do not significantly differ from the direction of cluster C1 (N60°E). This uncertainty on the dip of the fault plane makes it difficult to trace the position of the Loriaz fault at the surface precisely. The measured direction of the Loriaz fault parallels a set of small faults in the core of the Aiguilles Rouges massif, west of and oblique to the Remuaz fault (Fig. 10). The top of the aftershock zone its located at a depth of 4.5 km below the ground surface, making its correlation with surface faults difficult. It is also possible that the Loriaz fault is a hidden fault without any extension to the surface. However, it is tempting to associate the Loriaz fault plane at depth with one of the several small faults visible at the surface. Incidentally, field investigations by one of us (M. C.) have revealed small ground fissures in a sedimentary slope at the bottom of a long fracture striking N60°E and descending from the summit of the Gros Nol peak (Fig. 11). Field observations, combined with aerial photographs, provide evidence of other fractures striking N60°E in the same zone. The main lineament, beginning a few hundred meters north of the Gros Nol and 1.4 km long, is drawn on the detailed geological map of von Raumer and Bussy (2004) as a tectonic line. However, if we assume a mean dip of 75° for the ruptured fault plane, its surface trace could correspond to the westward extension of a clear surface fault located 2 km further north that runs from the Cheval Blanc peak towards the Emosson lake and dam (Fig. 10). Von Raumer and Bussy (2004) mapped this fault extending eastward right to the dam's west bank and crossing it towards its east bank. This 4 km long fault offsets the pre-Mesozoic basement metamorphic rocks in an apparent right-lateral displacement.

The hypocenter of the Vallorcine earthquake is definitely not located on the Remuaz fault (Fig. 10) located 4 km to the south-east and investigated by Alasset (2005), Alasset et al. (2005), Cara et al. (2006), and Van der Woerd et al. (2006). Its focal mechanism, which corresponds to a strike-slip fault, seems at first sight to be incompatible with their assumed mechanism for the Remuaz fault, since its P-axis oriented N102°E is almost perpendicular to the Remuaz fault. On the other hand, the Vallorcine mechanism agrees well with the assumed transpressive state of stress of the external zone attested to by several recent studies (e.g. Maurer et al. 1997, Sue et al. 1999, Delacou et al. 2004, Kastrup et al. 2004, Thouvenot and Fréchet 2005). Figure 12 presents all previously published reliable fault plane solutions in the region. The transpressive regime of the external zone is observed for a large number of

earthquakes in the neighbouring regions of the Mont Blanc and Aiguilles Rouges massifs. Several recent observations confirm this regime, be it the aforementioned broadly felt earthquakes of Grand-Bornand 1994 and Epagny 1996, the two Chablais events in 1990 and 2000 studied by Delacou et al. (2005), or the smaller 2001 sequence in the region of Martigny (Deichmann et al. 2002), which all exhibit strike-slip motion—with a small component of thrust for some of them. It is not uninteresting to observe that the difference between external and internal zones is not only exhibited by the stress regime, but also by the seismic regime. Indeed, as noted in the introduction, the internal zones are characterized by a lack of major historical earthquakes despite the strong activity of small magnitude earthquakes, almost the reverse of the external zones (Fig. 1).

Two hypotheses could explain the assumed conflicting motion on the Remuaz fault. The strike-slip mechanism of the Loriaz fault combined with the normal mechanism of the Remuaz fault may suggest that the Aiguilles Rouges massif is in a transtensive stress state, thus corresponding to a transition zone between the transpression in the external zone and the extension in the internal one. A similar apparent discrepancy was observed by Baer et al. (2003) in the Swiss Valais. Alternatively, the scarp with apparent normal faulting mapped by Alasset et al. (2005) on the Remuaz fault may correspond to a local gravitational slope instability or a postglacial differential uplift as modelled by Ustaszewski et al. (2008) in Switzerland. In the latter case, the Remuaz fault would not be the source zone of the Chamonix 1905 earthquake. Instead, the Chamonix 1905 event might have occurred on the same fault system as the Vallorcine 2005 earthquake. Re-evaluation of historical seismograms and bulletin data is necessary to find new evidence in favour of either hypothesis.

Acknowledgements

The field experiment benefited from a financial support by Institut National des Sciences de l'Univers (CNRS). We thank the field teams that helped to install and maintain the temporary network. Thanks to the two reviewers for their helpful suggestions. The Réseau National de Surveillance Sismique (RéNaSS), the Observatoire de Grenoble, and several Conseils généraux (Isère, Alpes-de-Haute-Provence, Hautes-Alpes, Haute-Savoie, Savoie, Ain) support the running costs of French seismic stations in the study area.

References

Alasset PJ (2005) Sismotectonique et identification des sources sismiques en domaine à déformation lente: cas des Pyrénées orientales et des Alpes du Nord (France); Le Tsunami créé par le séisme de Zemmouri (Mw=6.9, Algérie) du 21 mai 2003. Thèse de doctorat de l'Université Louis Pasteur, Strasbourg

Alasset PJ, Van der Woerd J, Cara M, Meghraoui M, Mériaux AS (2005) An active normal fault NW of the Mont Blanc massif, France: sign of extensive tectonics near the main thrust zone of the Chamonix valley? Eos Trans. AGU, 86(52), American Geophysical Union Fall Meeting 2005, Suppl., Abstract T51C-1356

Aki K, Richards PG (1980) Quantitative Seismology: Theory and Methods, vol 1. Freeman, San Francisco

Ayrton S, Barféty JC, Bellière J, Gubler Y, Jemelin L (1987) Feuille Chamonix, Carte géologique de la France à 1/50000. BRGM, Orléans

Baer M, Deichmann N, Braunmiller J, Bernardi F, Cornou C, Fäh D, Giardini D, Huber S, Kästli P, Kind F, Kradolfer U, Mai M, Maraini S, Oprsal I, Schler T, Schorlemmer D, Sellami S, Steimen S, Wiemer S, Wössner J, Wyss A (2003) Earthquakes in Switzerland and surrounding regions during 2002. Eclogae Geol Helv 96:313–324

Baer M, Deichmann N, Braunmiller J, Husen S, Fäh D, Giardini D, Kästli P, Kradolfer U, Wiemer S (2005) Earthquakes in Switzerland and surrounding regions during 2004. Eclogae Geol Helv 98:407–418

BCSF (2005) Séisme de Vallorcine (Savoie) du 8 septembre 2005. Note préliminaire BCSF2005-NP4. BCSF, Université de Strasbourg. http://www.franceseisme.fr/donnees/intensites/2005/050908_1127/050908_NotePreli_Vallorc_Part1.pdf. Accessed 11 March 2010

Cara M, Alasset PJ, Rivera L, Van der Woerd J, Fréchet J (2006) The Chamonix, 1905, earthquake: focal mechanism determination based on two Göttingen Wiechert records. 30th General Assembly of the ESC, Geneva (Switzerland)

Cara M, Schlupp A, Sira C (2007) Observations sismologiques: sismicité de la France en 2003, 2004, 2005. Bureau Central Sismologique Français, ULP/EOST – CNRS-INSU, Université de Strasbourg

Cara M, Alasset PJ, Sira C (2008) Magnitude of historical earthquakes, from macroseismic data to seismic waveform modelling: Application to the Pyrenees and a 1905 earthquake

in the Alps. In: Fréchet J, Meghraoui M, Stucchi M (eds.) Historical Seismology: Interdisciplinary Studies of Past and Rrecent Earthquakes, Springer, pp 369–384

Deichmann N, Baer M, Braunmiller J, Ballarin Dolfin D, Bay F, Delouis B, Fäh D, Giardini D, Kastrup U, Kind F, Kradolfer U, Künzle W, Röthlisberger S, Schler T, Salichon J, Sellami S, Spühler E, Wiemer S (2000) Earthquakes in Switzerland and surrounding regions during 1999. Eclogae Geol Helv 93:395–406

Deichmann N, Baer M, Braunmiller J, Ballarin Dolfin D, Bay F, Bernardi F, Delouis B, Fäh D, Gerstenberger M, Giardini D, Huber S, Kradolfer U, Maraini S, Oprsal I, Schibler R, Schler T, Sellami S, Steimen S, Wiemer S, Wössner J, Wyss A (2002) Earthquakes in Switzerland and surrounding regions during 2001. Eclogae Geol Helv 95:249–261

Deichmann N, Baer M, Braunmiller J, Cornou C, Fäh D, Giardini D, Gisler M, Huber S, Husen S, Kästli P, Kradolfer U, Mai M, Maraini S, Oprsal I, Schler T, Schorlemmer D, Wiemer S, Wössner J, Wyss A (2004) Earthquakes in Switzerland and surrounding regions during 2003. Eclogae Geol Helv 97:447–458

Deichmann N, Baer M., Braunmiller J, Husen S, Fäh D, Giardini D, Kästli P, Kradolfer U, Wiemer S (2006) Earthquakes in Switzerland and surrounding regions during 2005. Eclogae Geol Helv 99:443–452

Delacou B, Sue C, Champagnac JD, Burkhard M (2004) Present-day geodynamics in the bend of the western and central Alps as constrained by earthquake analysis. Geophys J Int 158:753–774

Delacou B, Deichmann N, Sue C, Thouvenot F, Champagnac J-D, Burkhard M (2005) Active strike-slip faulting in the Chablais area (NW Alps) from earthquake focal mechanisms and relative locations. Eclogae Geol Helv 98:189–199

Delouis B (2005) Le séisme du 8 septembre 2005 (11h27 UTC) à la frontière franco-suisse (Vallorcine). http://www-geoazur.unice.fr/SEISME/Mecaf_Vallorcine_RAP.jpg. Accessed September 2005 http://www.bcsf.prd.fr/donnees/intensites/2005/050908_1127/Mecaf_Vallorcine_RAP.jpg. Accessed 11 March 2010

Delouis B, Drouet S, Cara M, Nechtschein S, Lesueur C, Sylvander M, Souriau A, Sèbe O, Tocheport A (2008) Groupe de travail: magnitude de moment. RAP-Info 8:6–11

Delouis B, Charléty J, Vallée M (2009) A method for rapid determination of moment magnitude Mw for moderate to large earthquakes from the near-field spectra of strong-motion records (MWSYNTH). Bull Seismol Soc Am 99:1827–1840

ECOS (2009) Earthquake Catalog of Switzerland. Swiss Seismological Service. http://histserver.ethz.ch/intro_e.html. Accessed 11 March 2010

Fréchet J (2005) Hypref. http://sismalp.obs.ujf-grenoble.fr/ftp-sismalp/unix. Accessed 11 March 2010

Fréchet J, Thouvenot F, Jenatton L, Hoang-Trong P, Frogneux M (1996) Le séisme du Grand-Bornand (Haute-Savoie) du 14 décembre 1994: un coulissage dextre dans le socle subalpin. C R Acad Sci Paris 323:517–524

Fréchet J, Thouvenot F (2004) Pickev 2000: Software for seismogram picking and processing, earthquake location, and mapping. http://sismalp.obs.ujf-grenoble.fr/ftp-sismalp/msdos. Accessed 11 March 2010

Global CMT. Global Centroid-Moment-Tensor (CMT) Project. http://www.globalcmt.org. Accessed 11 March 2010

Kastrup U, Zoback ML, Deichmann N, Evans K, Giardini D, Michael AJ (2004) Stress field variations in the Swiss Alps and the northern Alpine foreland derived from inversion of fault plane solutions. J Geophys Res 109. doi:10.1029/2003JB002550

Lee WHK, Lahr JC (1975) HYP071 (Revised): A computer program for determining hypocenter, magnitude, and first motion pattern of local earthquakes. U. S. Geological Survey Open File Report 75-311

Leloup PH, Arnaud N, Sobel ER, Lacassin R (2005) Alpine thermal and structural evolution of the highest external crystalline massif: The Mont Blanc. Tectonics 24, TC4002. doi:10.1029/2004TC001676.

Maurer HR, Burkhard M, Deichmann N, Green AG (1997) Active tectonism in the central Alps: contrasting stress regimes north and south of the Rhone Valley. Terra Nova 9:91–94

Pfiffner OA, Lehner P, Heitzmann P, Mueller S, Steck A (1997) Deep Structure of the Swiss Alps: Results of NRP 20. Birkhäuser, Basel

SED (2005a) Swiss Moment Tensor Solutions 2005. http://www.seismo.ethz.ch/moment_tensor/2005/homepage.html. Accessed 11 March 2010

SED (2005b) Annual seismicity report of the swiss seismological service 2005. http://histserver.ethz.ch/seismotectonics/reports/2005.pdf. Accessed 11 March 2010

Sellami F, Kissling E, Thouvenot F, Fréchet J (1995) Initial reference velocity model for seismic tomography in the western Alps. 20th Gen. Ass. EGS, Hamburg

SisFrance (2010) Base de données de sismicité historique française. BRGM, EDF, IRSN. http://www.sisfrance.net. Accessed 11 March 2010

Sue C, Thouvenot F, Fréchet J, Tricart P (1999) Widespread extension in the core of the western Alps revealed by earthquake analysis. J Geophys Res 104:25611–25622

Thouvenot F, Fréchet J, Tapponnier P, Thomas J-C, Le Brun B, Ménard G, Lacassin R, Jenatton L, Grasso J-R, Coutant O, Paul A, Hatzfeld D (1998) The ML 5.3 Épagny (French Alps) earthquake of 1996 July 15: a long-awaited event on the Vuache fault. Geophys J Int 135:876–892

Thouvenot F, Fréchet J, Jenatton L, Gamond J-F (2003) The Belledonne Border Fault: identification of an active seismic strike-slip fault in the western Alps. Geophys J Int 155:174–192

Thouvenot F, Fréchet J (2005) Seismicity along the northwestern edge of the Adria microplate. In: Pinter et al. (eds.) The Adria Microplate: GPS Geodesy, Tectonics and Hazards, Kluwer, pp 335–349

Ustaszewski ME, Hampel A, Pfiffner OA (2008) Composite faults in the Swiss Alps formed by the interplay of tectonics, gravitation and postglacial rebound: an integrated field and modelling study. Swiss J Geosci 101:223–235

Van der Woerd J, Alasset PJ, Cara M, Meghraoui M, Rivera L (2006) The Remuaz fault in the Aiguilles Rouges massif (France): evidence for an active normal fault NW of the Mont Blanc? EGU General Assembly, Vienna, Austria, Geophys Res Abstr 8:3719

Von Raumer JF, Bussy F (2004) Mont Blanc and Aiguilles Rouges: Geology of their polymetamorphic Basement (External Massifs, France-Switzerland). Mémoires de Géologie (Lausanne) 42

Waldhauser F (2001) HypoDD – A Program to Compute Double-Difference Hypocenter Locations. U. S. Geological Survey Open File Report 01-113

Waldhauser F, Ellsworth WL (2000) A double-difference earthquake location algorithm: Method and application to the northern Hayward fault. Bull Seismol Soc Am 90:1353–1368

Wells DL, Coppersmith KJ (1994) New empirical relationships among magnitude, rupture length, rupture width, rupture area, and surface displacement. Bull Seismol Soc Am 84:974–1002

Tables

Agency	Time	Latitude N	Longitude E	Depth km	M_L	M_D/M_W
LDG	11:27:18.29	46.033	6.958	2	5.3	4.5 M_D
RENASS	11:27:18.57	46.03	6.89	10	4.9	
SED	11:27:17.4	46.032	6.897	8	4.9	4.5 M_W
SISMALP	11:27:16.83	46.024	6.937	-1.8	4.6	
(this study)	11:27:18.09	46.038	6.889	4.34		

Table 1 Locations of the mainshock

	Strike	Dip	Rake
Plane 1	**60°**	**65°**	**-180°**
Plane 2	150°	90°	-25°
	Trend	Plunge	
P axis	282°	18°	
T axis	17°	18°	

Table 2 Focal-solution parameters for the mainshock. Strike, dip, and rake as defined by Aki and Richards (1980). Focal depth at 5.1 km. Velocity model by Sellami et al. (1995). Preferred fault plane in bold type

Institute	**Number of Stations**	**Recorder**	**Sensor**
IPGS	11	Geostar	Mark Products L4 (1 Hz) or L22 (2 Hz)
LGIT	6	Hathor Leas	Mark Products L22 (2 Hz)
LGIT	8	Minititan Agecodagis	Lennartz LE-3D/5s
SED	3	Quanterra	Lennartz LE-3D/5s

Table 3 Stations and sensors used in the temporary network

Cluster	Before Sept 2005	Sept–Dec 2005	After Dec 2005
C1	2001 (1) ML 1.0 2002 (2) ML 1.3–1.5 2004 (1) ML 0.6 2005 June (1) ML 0.9	Sept–Dec (57) ML 0.1–4.9	2006 (33) ML 0.5–1.5 2007 (16) ML 0.3–2.1 2008 (17) ML 0.1–2.6 2009 (17) ML 0.2–1.4
C2a		Sept (10) ML 0.4–2.2	
C2b		Oct–Dec (42) ML 0.4–1.9	2006 Jan (2) ML 0.5–0.9 2006 Aug–Oct (8) ML 0.5–1.7
C3	2000 (3) ML 1.4–1.6	Sept-Oct (4) ML 0.4–1.5	2006 (2) ML 0.8–2.1 2007 (1) ML 0.6

Table 4 Events detected by the permanent network of the SED during different time periods and associated with each cluster (number of events in parentheses)

Figure captions

Fig. 1 Situation map of the Vallorcine earthquake. Geology: grey = external Alps, pink = external crystalline massifs, yellow = internal Alps, orange = internal crystalline massifs. Seismicity: star = Vallorcine 2005 epicentre, red = microseismicity 1992–2004 from SED and Sismalp, open circles = historical earthquakes with intensity above VI, red open circles = Epagny and Grand-Bornand earthquakes (see text)

Fig. 2 Map of the temporary seismic network in operation between September 9 and October 10, 2005 (triangles) and the permanent stations (squares). Epicentre locations of the mainshock calculated routinely by the different seismological services shown as black dots

Fig. 3 Focal mechanism of the mainshock (lower hemisphere Schmidt projection). Full symbols: compression; open symbols: dilatation; symbol size is smaller when first motion is emergent. Preferred fault plane strikes N60°E, with a 65°SE dip

Fig. 4 Map of aftershocks recorded by the temporary network (absolute locations, computed with Hypref). C1 = main cluster; C2, C3, C4 = sub-clusters

Fig. 5 Transverse cross-section of aftershocks recorded by the temporary network (absolute locations). Depths relative to sea level. C1 = main cluster; C2, C3, C4 = sub-clusters

Fig. 6 Close-up view of the clusters (relative locations, computed with HypoDD): a) map; b) longitudinal cross-section A–A'; c) transverse cross-section B–B'. C1 = main cluster; C2, C3, C4 = sub-clusters

Fig. 7 Map of the whole foreshock–mainshock–aftershock sequence (relative locations). Black dots = aftershocks located during the temporary-network period, green circles = foreshocks, large red circle = mainshock, small red circles = early aftershocks, blue circles = late aftershocks. Symbol size is not significant. C1 = main cluster; C2, C3, C4 = sub-clusters

Fig. 8 Transverse time-section BB' (see Fig. 6a) including foreshocks, mainshock, and two-month aftershock sequence. Dotted line = day of the mainshock (8 September 2005); star = mainshock. C1 = main cluster; C2, C3, C4 = sub-clusters

Fig. 9 Examples of seismograms recorded at the permanent station SALAN, 14 km NNE of the epicentral zone (ground velocity, vertical component, band-pass filtered 1–20 Hz): a) five signals of a family of almost identical events within cluster C1 recorded in 2001, 2005, 2006, 2007 and 2009; b) two signals of cluster C2a in 2005 (top) and three signals of cluster C2b in 2005 and 2006 (bottom). Date, time (UTC) and magnitude (ML) are listed above each trace, and maximum amplitude (nm/s) below

Fig. 10 Tectonic setting of the Vallorcine earthquake sequence. Dark grey = crystalline massifs (Mont Blanc and Aiguilles Rouges); light grey = autochthonous terrain (Mesozoic cover). Thick lines = faults (modified from Ayrton et al. 1987); dashed line = French-Swiss border. Fault mechanism shown for the Remuaz fault (Alasset et al. 2005) and the Mont Blanc shear zone (MBsz) (Leloup et al. 2005); dip direction and kinematics of the other faults are unknown

Fig. 11 Gros Nol peak viewed from the northeast, exhibiting strong fracturing striking N60°E, i.e. parallel to the Vallorcine rupture plane. Top and bottom of fracture shown by red lines. Minute fresh surface fissures, which are probably incidental, were observed in the gravel bank at the bottom of the cliff. The altitudes of the top and bottom of the Gros Nol are shown. (Photograph M. Cara)

Fig. 12 Seismotectonic map showing reliable fault plane solutions in the region (1980–2005). Data taken from Fréchet et al. (1996), Thouvenot et al. (1998), Sue et al. (1999), Deichmann et al. (2000), Deichmann et al. (2002), Baer et al. (2003), Thouvenot et al. (2003), Deichmann et al. (2004), Kastrup et al. (2004), Baer et al. (2005), Delacou et al. (2005). Fault plane solution of the Vallorcine earthquake is shown in red. Otherwise, same as Fig. 1

colour figure

Click here to download high resolution image

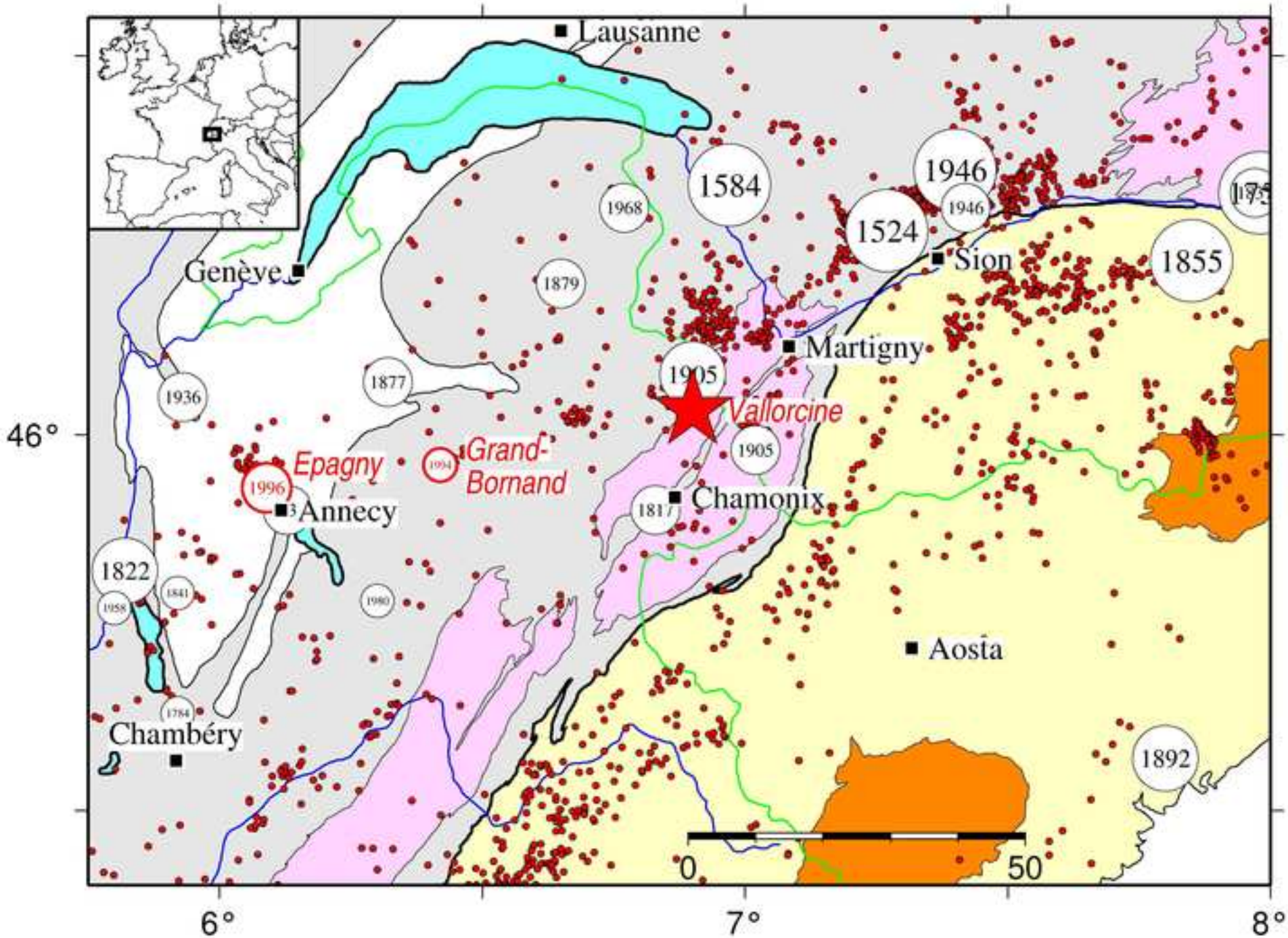

colour figure
Click here to download high resolution image

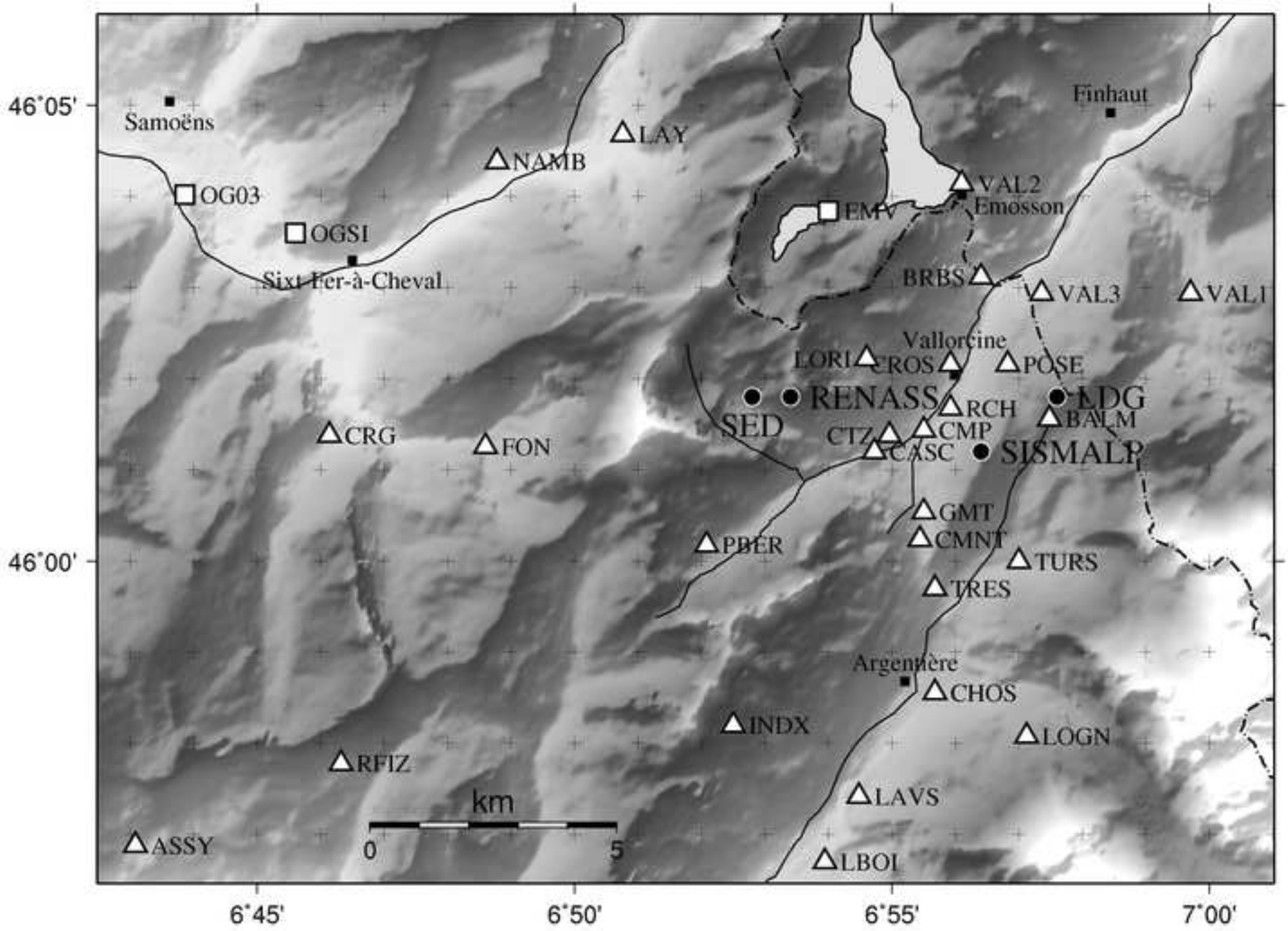

colour figure

Click here to download colour figure: Fig3.ps

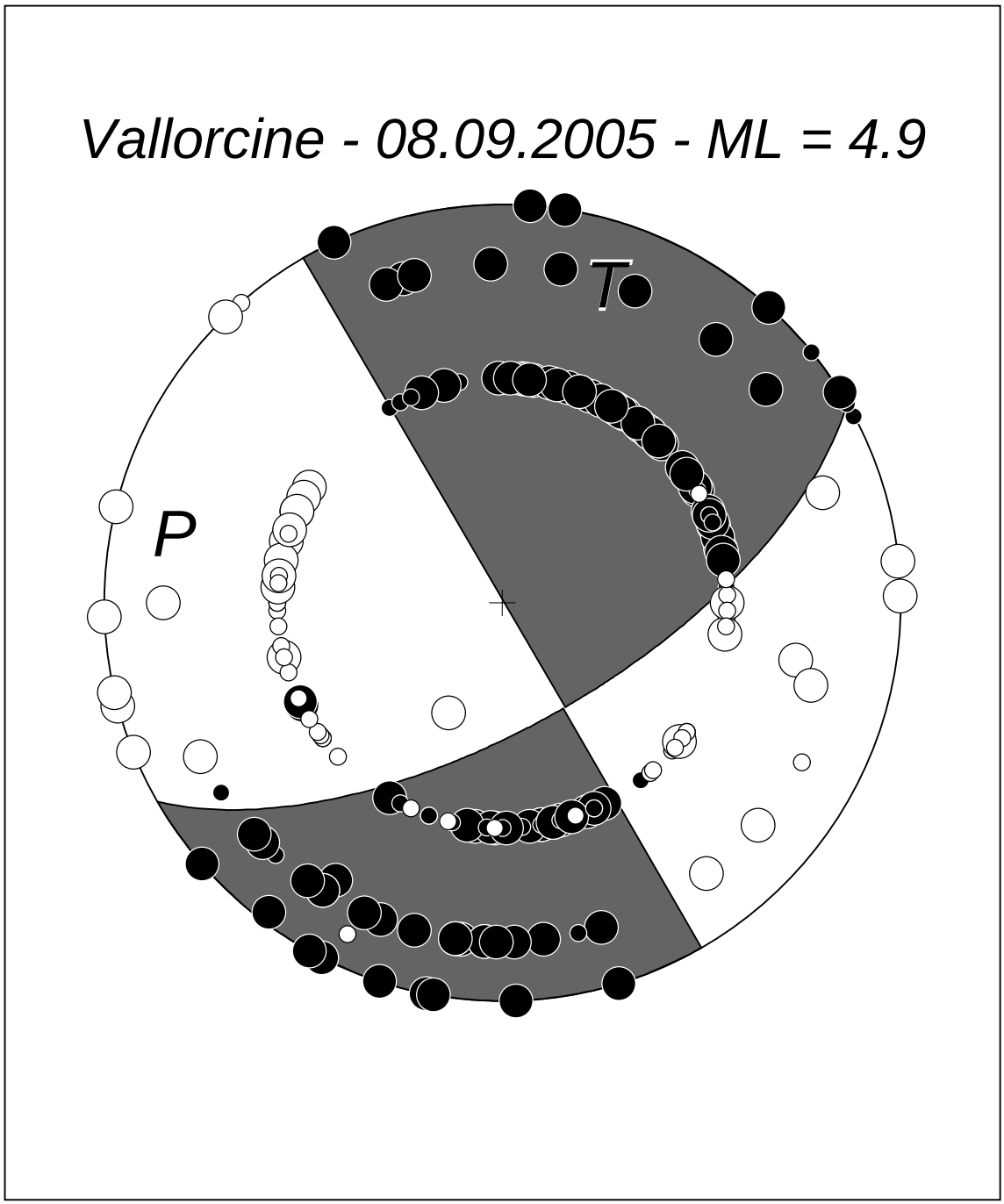

colour figure

Click here to download high resolution image

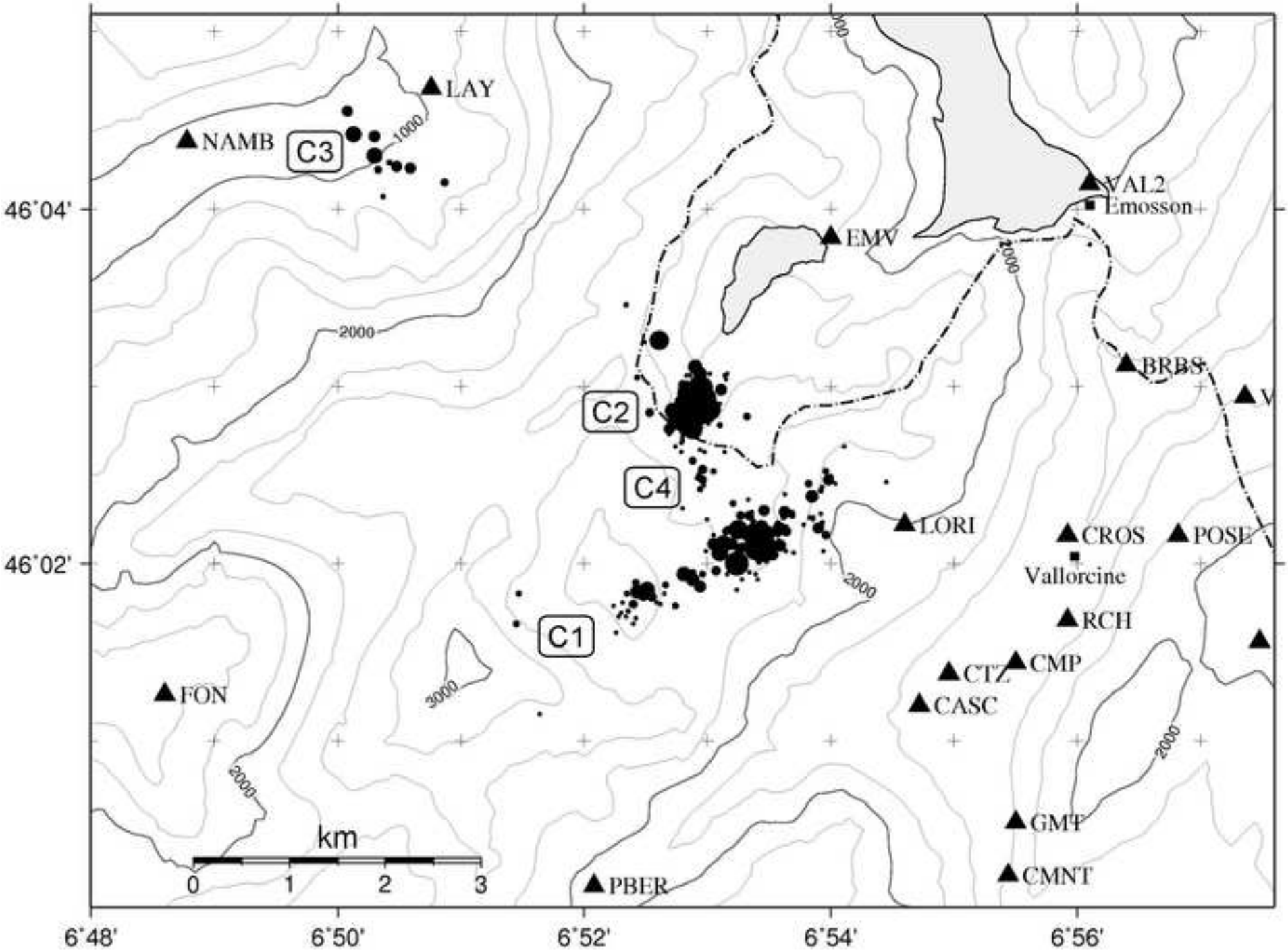

colour figure
Click here to download high resolution image

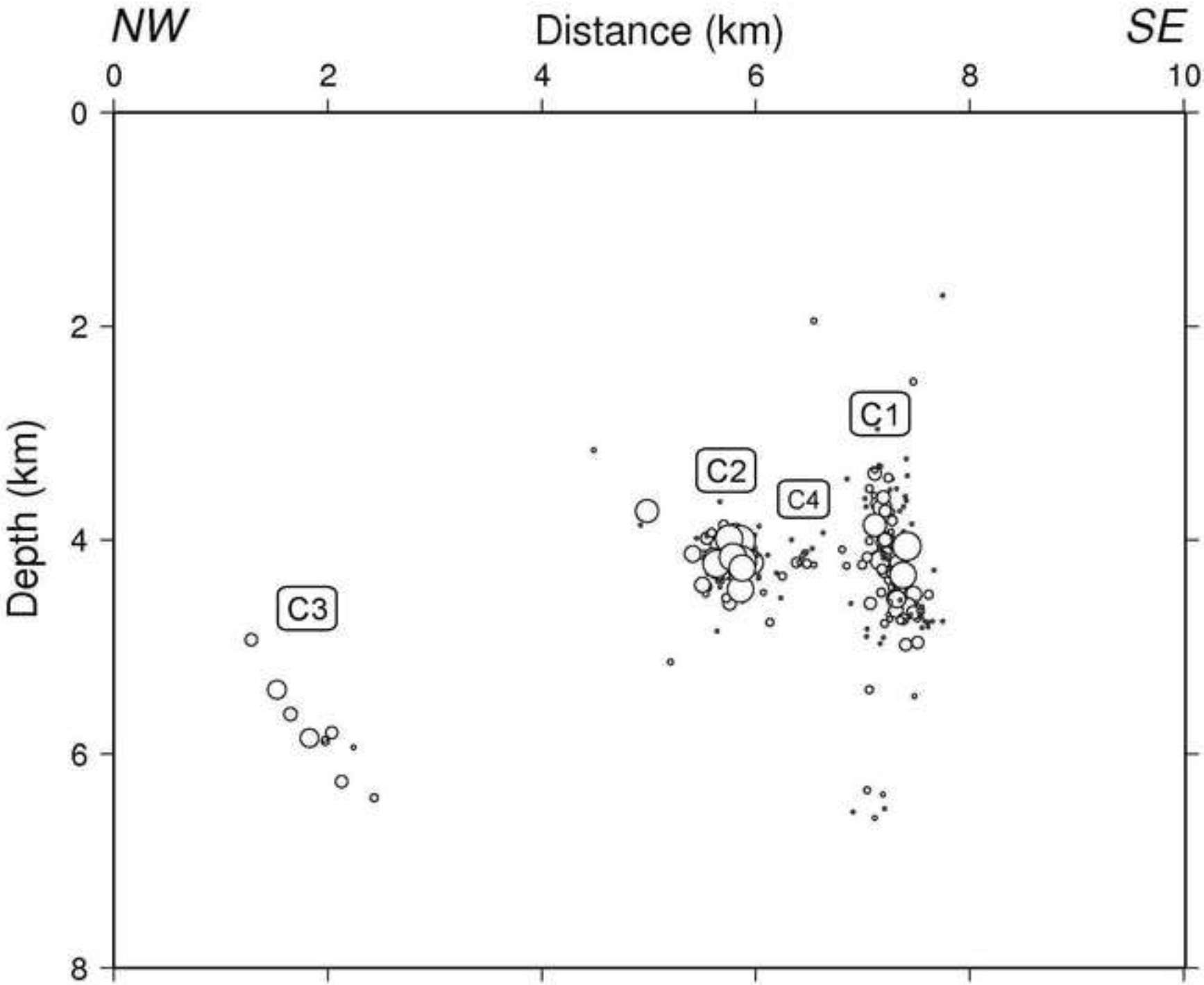

colour figure
Click here to download high resolution image

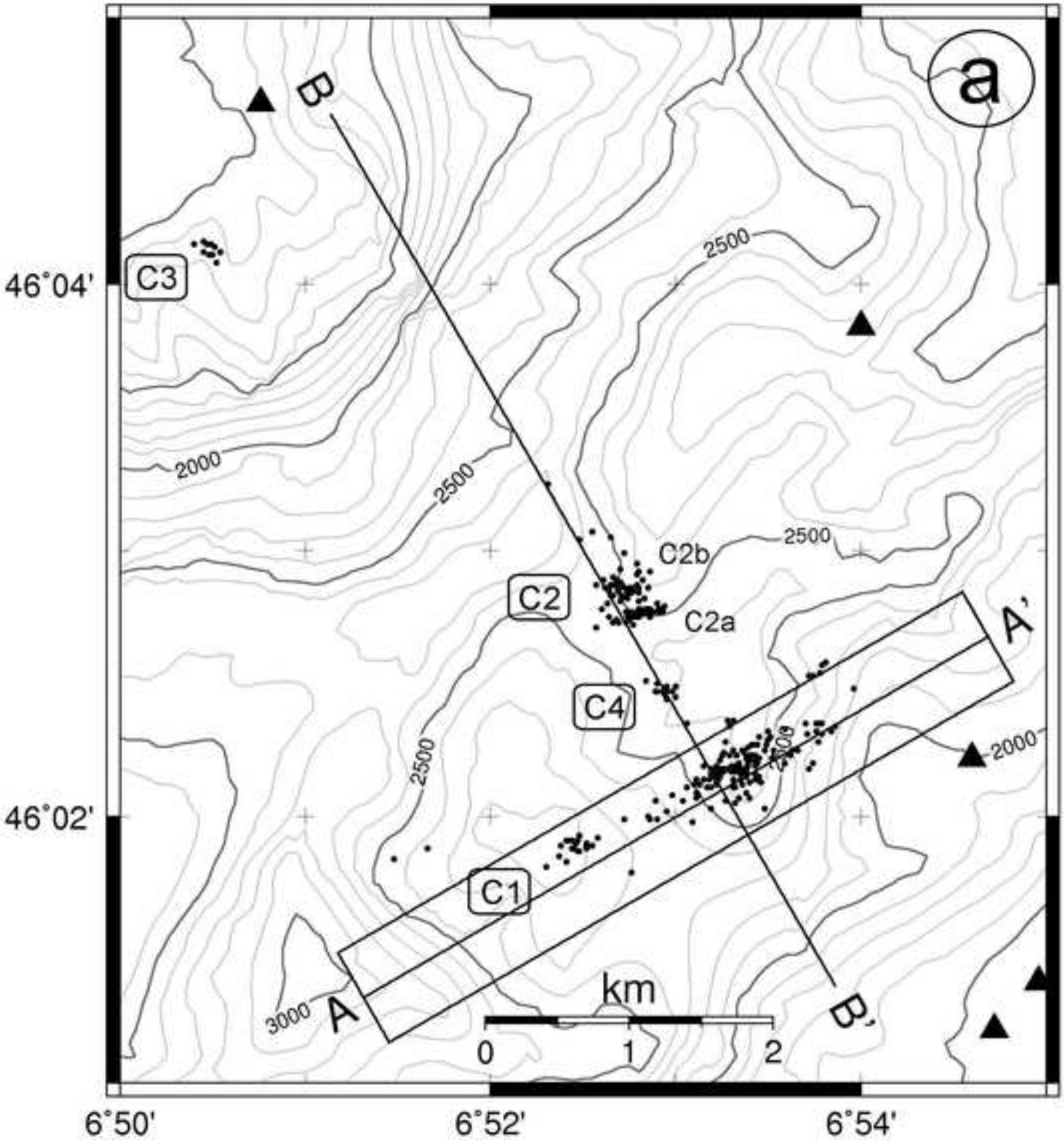

colour figure
Click here to download high resolution image

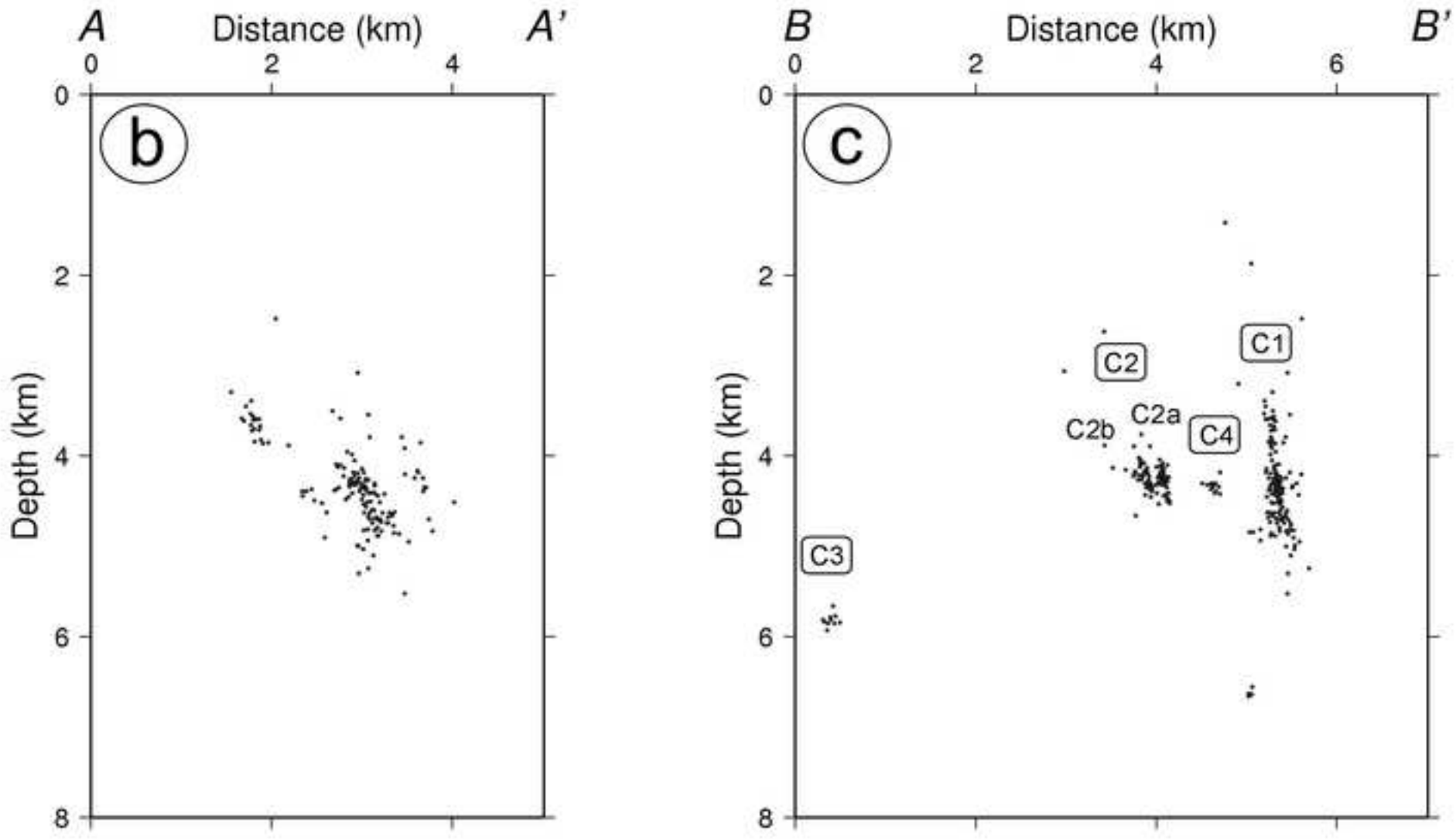

colour figure
Click here to download high resolution image

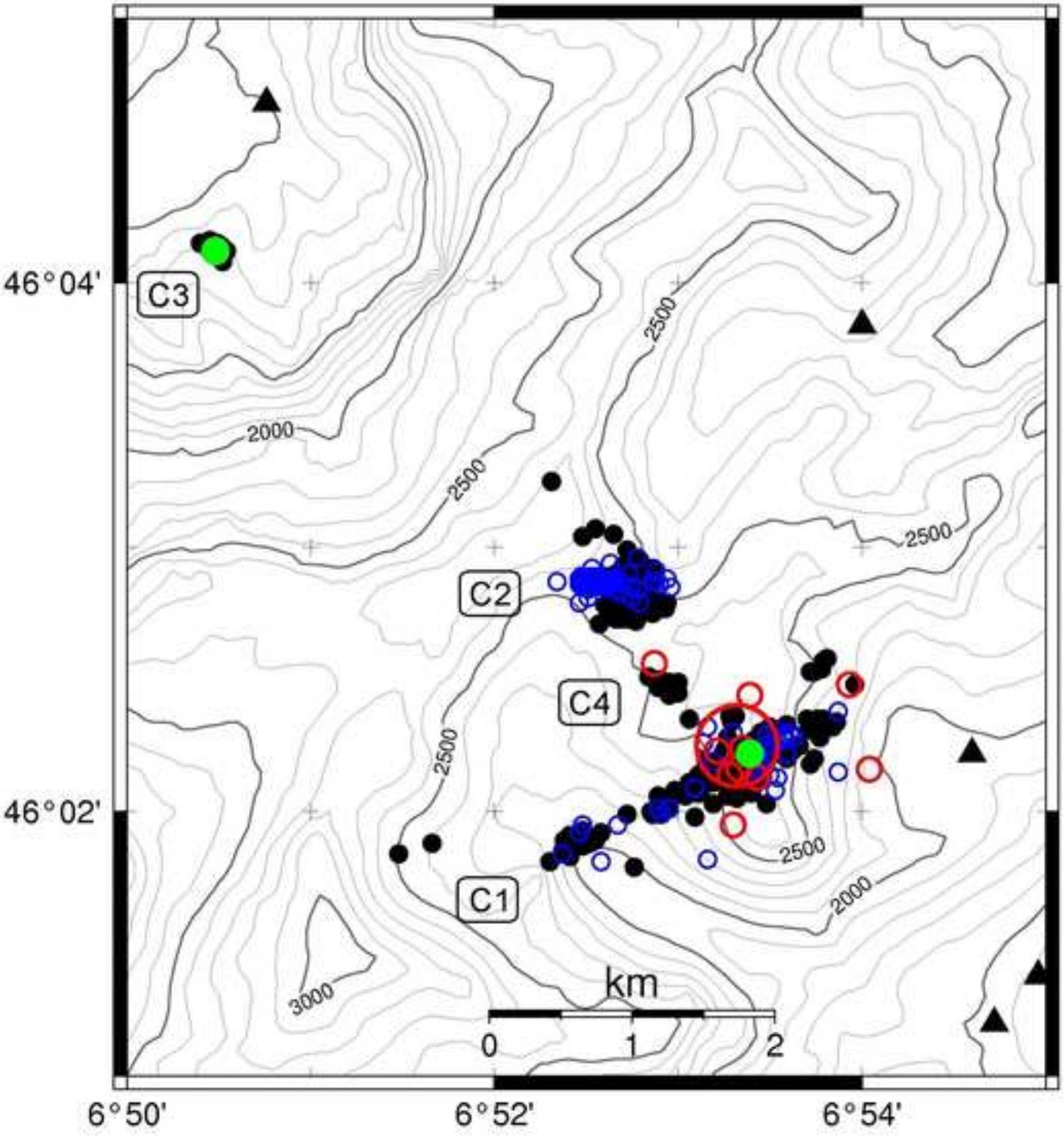

colour figure
Click here to download high resolution image

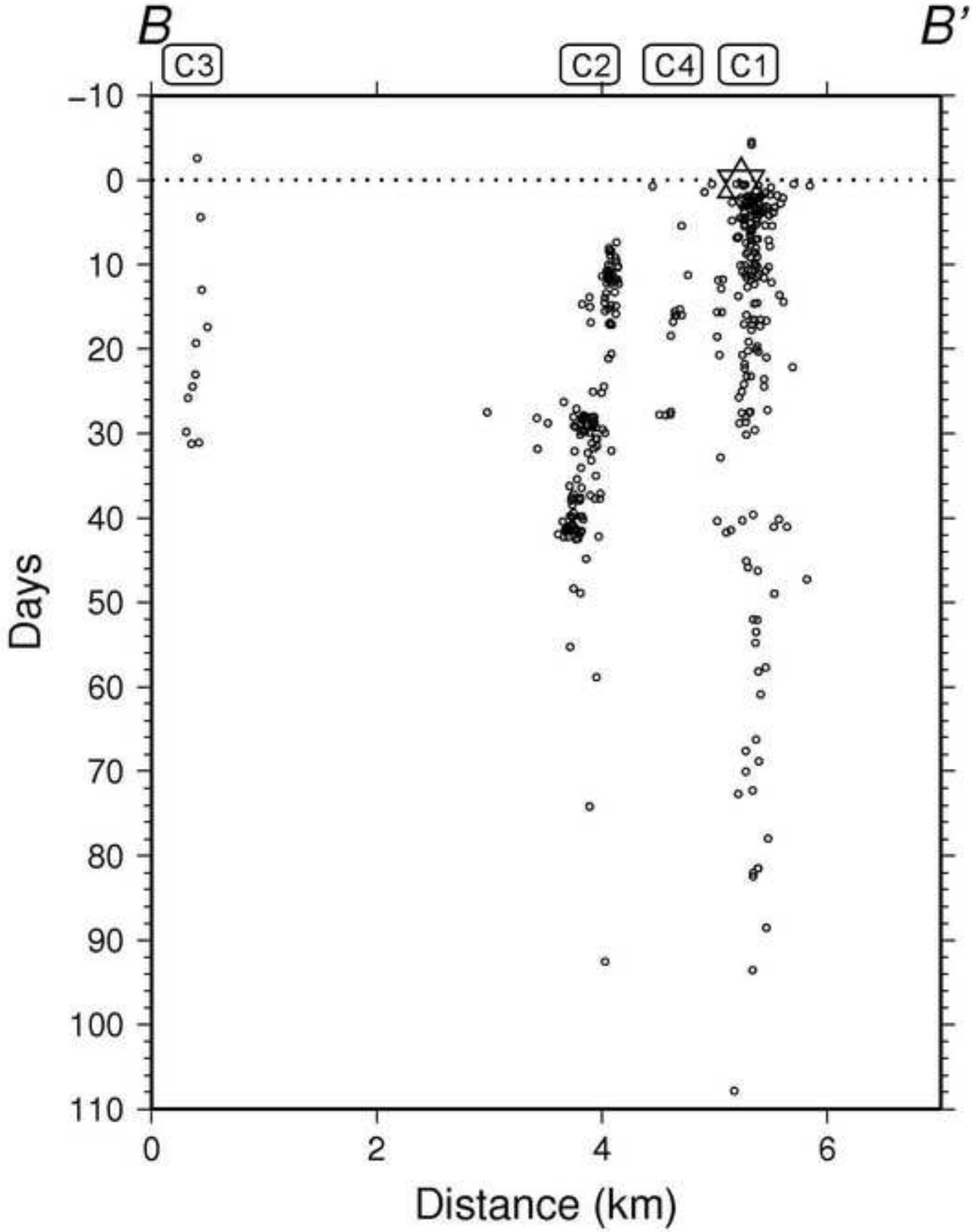

colour figure
Click here to download colour figure: Fig9.eps

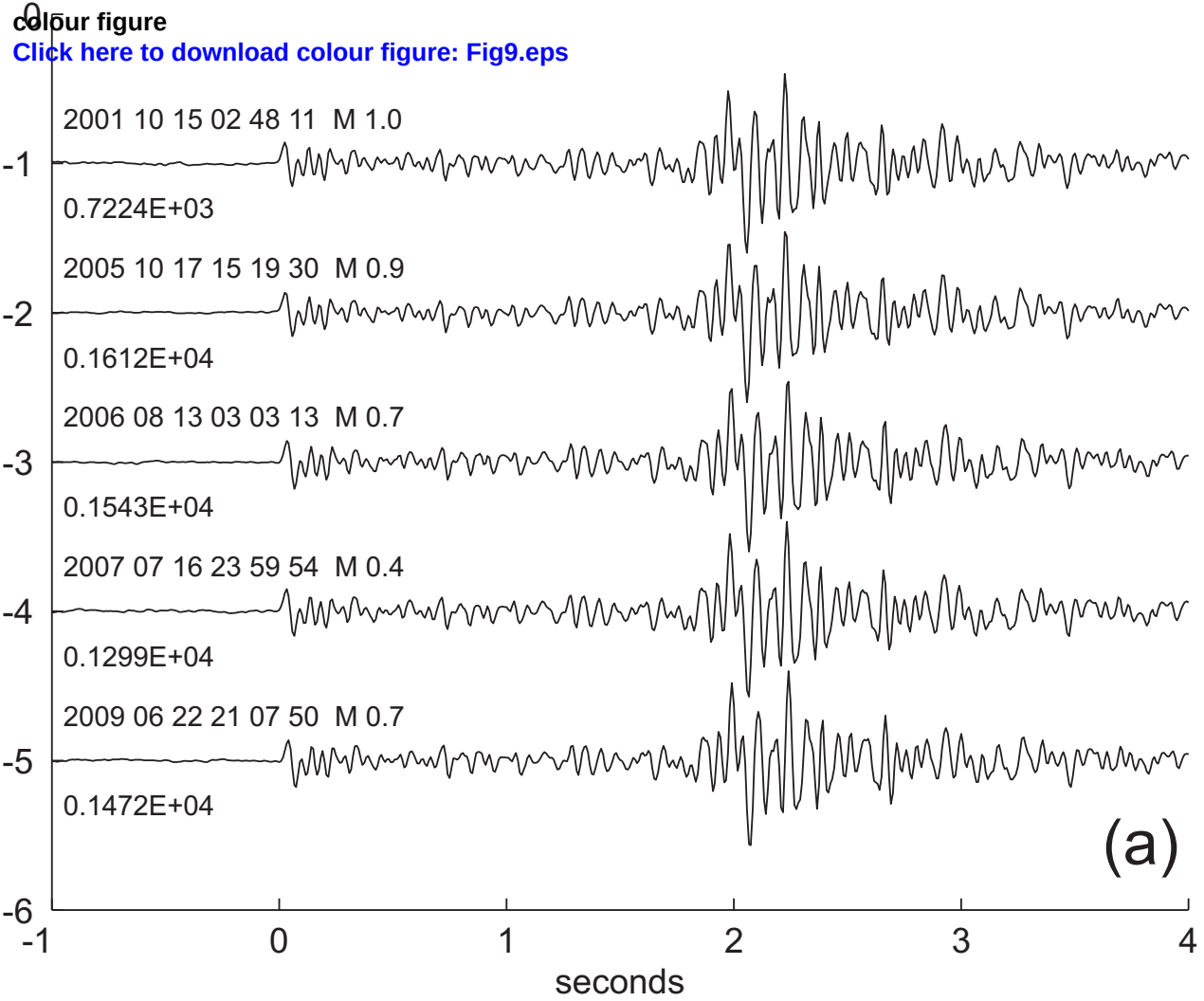

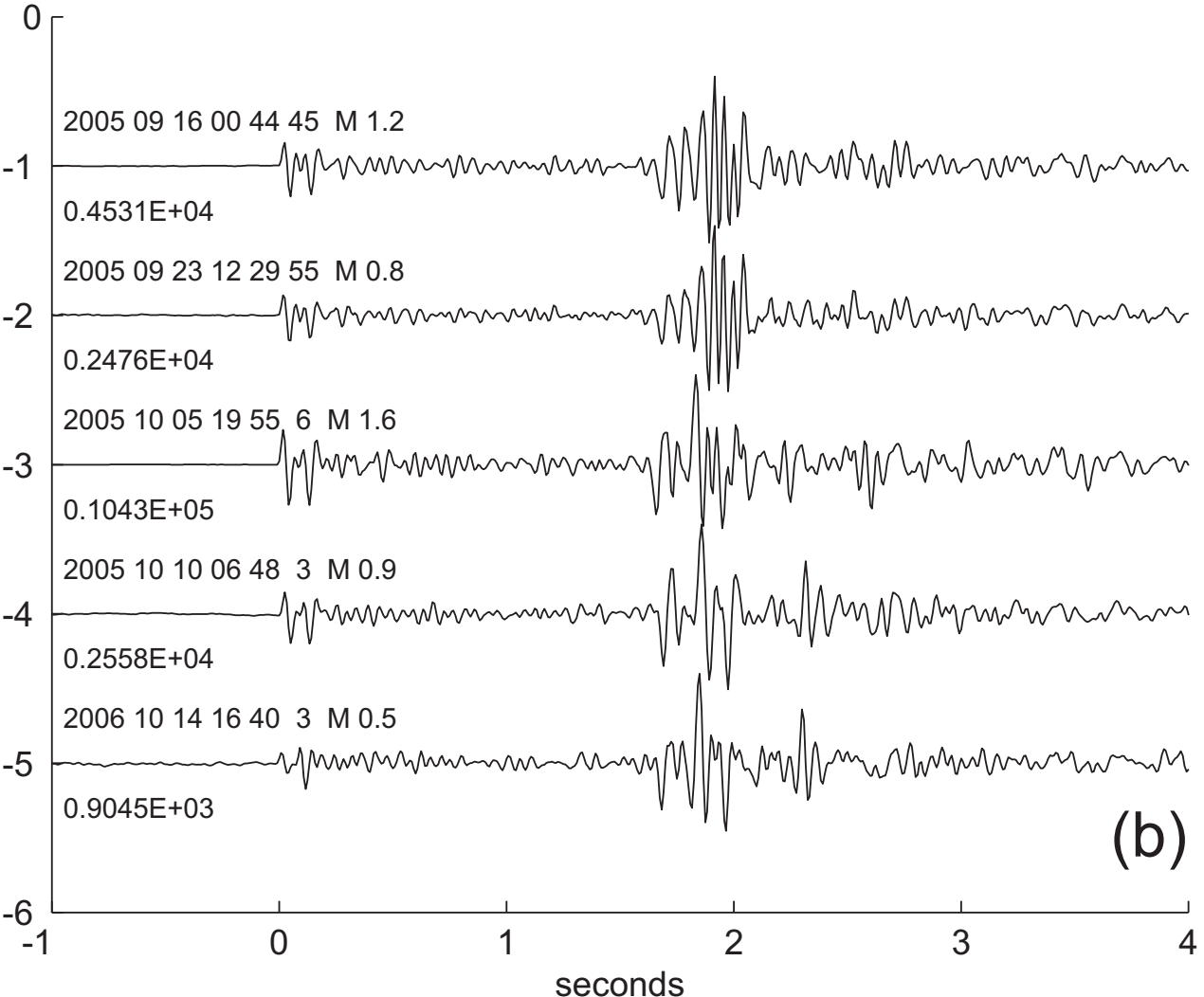

colour figure
Click here to download high resolution image

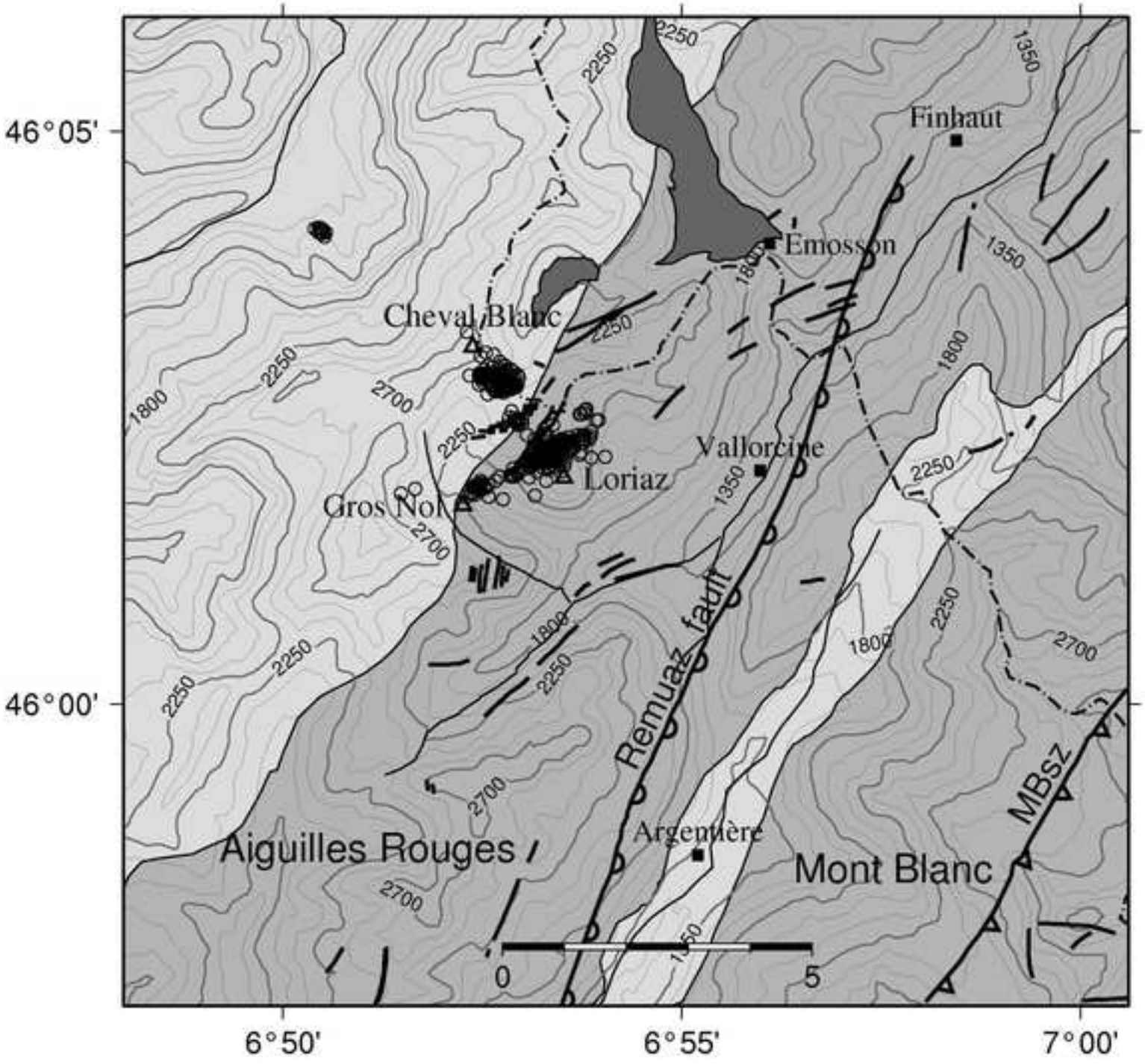

colour figure
Click here to download high resolution image

colour figure
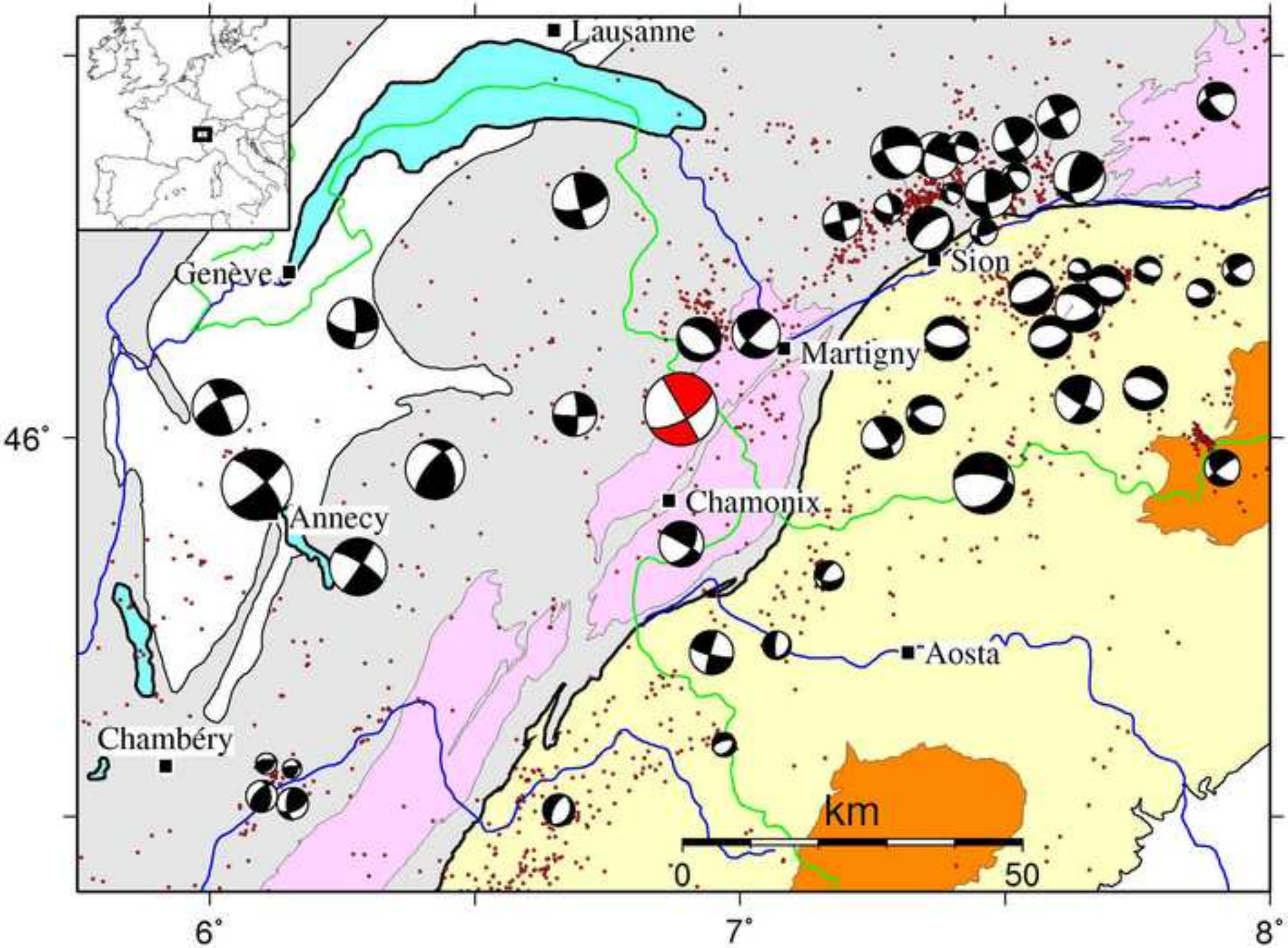
Click here to download high resolution image